# Flexible Substrate Technology for Millimeter Wave Wireless Power Transmission

Zhening Yang, Alexandru Takacs, Samuel Charlot, Daniela Dragomirescu

# Flexible Substrate Technology for Millimeter Wave Wireless Power Transmission

Zhening Yang[1,2], Alexandru Takacs[1,3], Samuel Charlot[1], Daniela Dragomirescu[1,2]

[1] CNRS, LAAS, 7 Avenue du Colonel Roche, F-31400 Toulouse, France

[2] Univ de Toulouse, INSA, LAAS, F-31400 Toulouse, France

[3] Univ de Toulouse, UPS, LAAS, F-31400 Toulouse, France

In this paper, a technology based on thin flexible polyimide substrate (Kapton) to develop antennas for millimeter wave wireless power transmission is presented. Firstly, we characterize the Kapton polyimide (relative permittivity and loss tangent) by using a ring resonator method up to V band. A 60 GHz patch antenna is designed, fabricated, and measured to validate our technology. Crossed dipoles array antennas at Ku band and K band for energy harvesting are also designed, fabricated and measured. Then a prototype of crossed slot dipole antenna at V band is proposed. Finally, a resistivity characterization of Au bump used in flip chip packaging is done, which leads us one step further towards a heterogeneous integration on flexible substrate of different components for Wireless Sensor Network nodes.

Corresponding author email: daniela.dragomirescu@laas.com; phone: +33 5 61 33 63 79

## I. INTRODUCTION

There is an increasing demand of high efficiency antennas and passives for applications where high frequency operation, lightweight, and conforming to a curved surface are required. Flexible electronics have spanned impressively over the past years, and flexible substrate became a strong competitor compared to his rigid counterparts because they are typically lighter, more rugged and portable, and less expensive to manufacture [1].

Table 1. Comparative properties of state-of-art flexible substrates [2].

| Material | PET | PEN | Kapton | LCP | Paper |
|---|---|---|---|---|---|
| **Mechanical properties** | Good | Good | Excellent | Good | - |
| **Heat resistance** | Low | Very good | Excellent | Good | - |
| **Chemical resistance** | Good | Good | Good | Excellent | - |
| **Electrical properties** | Good | Good | Good | Good | Good |

## A) Flexible substrate choice

The choice of flexible substrate for the applications at microwave frequencies is a challenge, because the substrate must exhibits good electrical (e.g. low losses), mechanical and chemical properties. Moreover, the substrate should keep these electrical properties over a wide range of frequencies and under external conditions such as temperature and pressure etc. Finally, substrates used in RF devices should be able to withstand the rigors (e.g. humidity, gasing) of their operating environment and of the fabrication processes used in their packaging [3].

Several flexible substrates used for printed circuit packaging are listed in Table 1, one can see the characterizations of polyethylene teraphthalate (PET) [4], polyethylene naphthalate (PEN) [5], Kapton [6], liquid crystal polymers (LCP) [3] and paper-based substrate [7]. LCP has a nearly constant relative permittivity of 3.1 and low loss (tan $\delta$ = 0.002-0.005) up to millimeter wave frequency range, along with a near-hermetic nature (water absorption < 0.04%) which make it suitable for high frequency designs. The paper based substrate is a good candidate thanks to its low cost, but it has limitations issues related to high frequency, absorption, and humidity. Finally, we selected Kapton as substrate for the development of our passive circuits due to its good RF and thermal properties, very good flexibility over a wide temperature range (-73°C to +400°C) and its resistance to many chemical solvents.

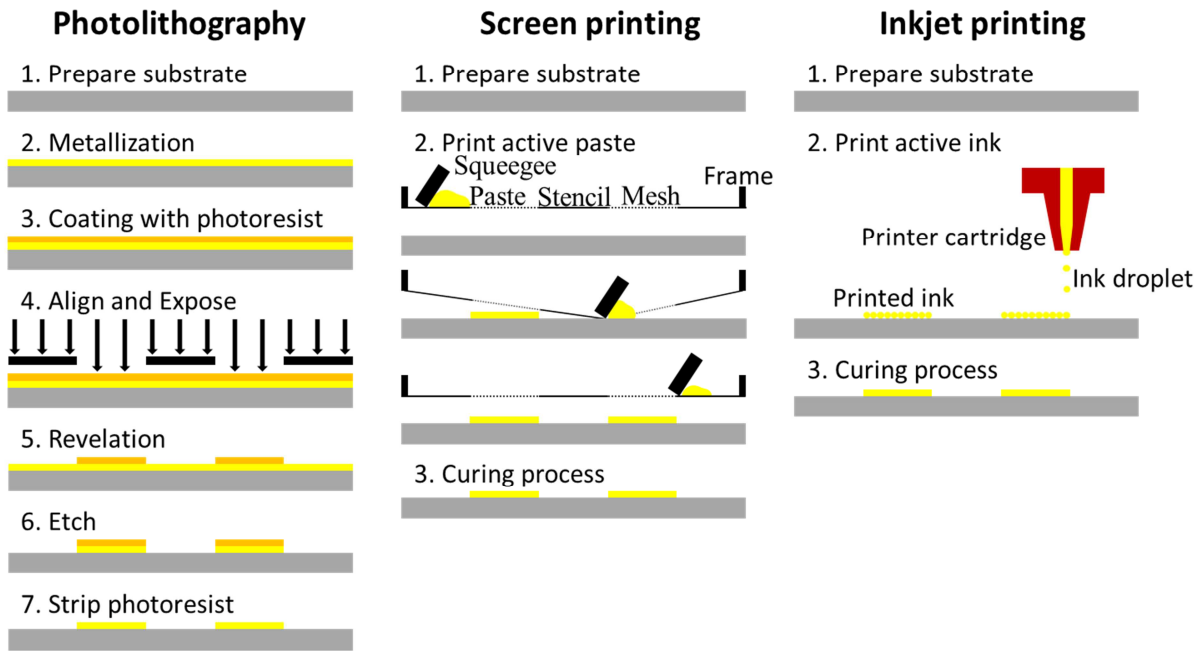


Fig. 1. Comparison of the processing steps involved in subtractive microfabrication, screen printing and inkjet printing [8].

## B) Process technology choice

The most widespread technologies used in microfabrication are photolithography, screen printing, and inkjet printing (Fig. 1). Inkjet printing is a direct write technology which presents a low cost advantage because the design pattern is transferred directly to the substrate

and does not require masks. However, the liquid metal nanoparticles used for inkjet printing have much lower conductivity compared to the bulk conductor used for lithography [9][10], which can degrade the printed circuit's performances at RF and millimeter wave frequency. In addition, millimeter wave applications require high accuracy, and both screen printing and inkjet printing can only offer a highest resolution around 20 μm [11]. Antennas fabricated on Kapton at lower frequency have been reported in [12] [13] by using screen printing or inkjet printing, but the traditional photolithography remains the most suitable method for microfabrication at millimeter frequency range.

This paper is organized as follows. The second chapter presents a description of the fabrication process we have developed, followed in the third chapter by a study of Kapton dielectric properties using a ring resonator method. Then, a design of a 60GHz grounded coplanar waveguide feeding patch antenna and two crossed dipoles array antennas at Ku band and K band are described. A prototype of crossed slot dipole antenna at V band is also analysed here. Finally, experimental results concerning the resistivity of Au bump used in flip chip packaging is presented.

## II. TECHNOLOGICAL PROCESS FOR FLEXIBLE SUBSTRATE INTEGRATION

To manufacture our circuits onto a flexible substrate, we have chosen the traditional photolithography, the main difficulty during the fabrication process lies on the flexible film handling and its use in micro-technology equipment. In order to overcome this difficulty, a 4-inch silicon wafer is used as a host carrier. One of the critical obstacles consists in finding a way to adhere the polyimide film on the Si support. This adhesion has to be compatible with the various technological stages (vacuum, solvent and temperature) and allows after manufacture a peeling without any physical or chemical constraint.

A matured fabrication process is used where first a PDMS (PolyDiMethylSiloxane) spin coating is performed for the adhesion of the polyimide on the holding wafer. Then the Kapton polyimide is patterned on the PDMS-Si support using a Shipley 360N laminator. A resin spin coating is then realized in a fully automated resist processing tool EVG120, followed by a photolithography process [14].

(a) (b)

Fig. 2. a) Shipley 360N Laminator; b) EVG120 resist processing system

During the different fabrication processes, Kapton polyimide is metallized with Ti/Au layers (50 nm/ 200 nm) or Ti/Cu layers (50 nm/500 nm) using the Electron Beam Physical Vapor Deposition (EBPVD). In case of Cu coating, the fabrication process will be terminated with a surface finishing (gold immersion deposits) to prevent Cu from oxidizing. Both wet-etching and lift-off methods were carried out during different tests, each of them is able to obtain a sufficient resolution for the metallization tracks.

The skin depths of gold and copper at microwave frequencies are given in Fig. 3. One can see the skin depth decrease with higher frequency. So with the metal thickness mentioned above, selected mainly for V-band applications, high losses at lower frequencies should be expected.

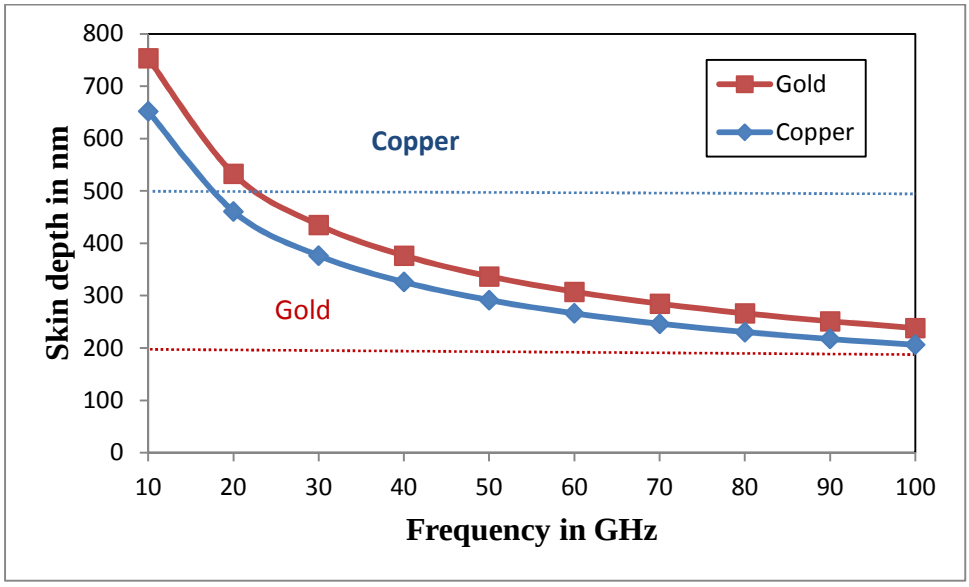


Fig. 3. Skin depth versus frequency, the horizontal lines show the selected metallization thickness

## III. CHARACTERIZATION OF KAPTON

A commercially 127-µm Kapton (type 500HN) was chosen as our flexible substrate, which is the thickest product available in the HN series. In fact there is a minimum substrate thickness that must be respected for designing an effective patch antenna in V-band. This antenna is composed by a rectangular patch on the top side of the substrate and a ground plane on the back side. In order to avoid undesired capacitive effect and to ensure a highly-efficient radiation mechanism of a patch antenna, a quick parametric study is done. It shows the influence of substrate thickness versus maximum antenna gain in HFSS simulation [15] (Fig. 4). One can see that the thicker the substrate, the better the antenna gain, regardless its metallization layer: Perfect Electric Conductor (PEC), copper or gold.

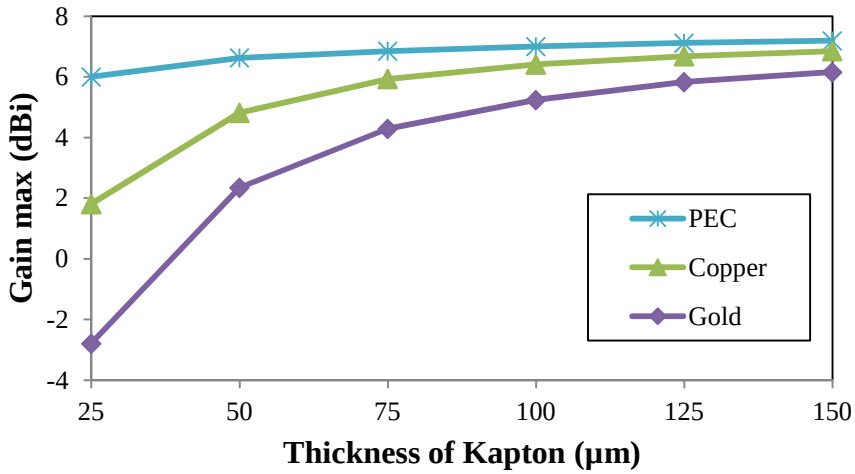


Fig. 4. Maximum simulated antenna gain versus substrate thickness at 60 GHz.

To design properly any high-frequency structure on this 127-µm Kapton by using numerical simulation, the knowledge of dielectric properties of substrate becomes necessary. The dielectric properties of Kapton: the relative permittivity $\varepsilon_r$ and the loss tangent tan $\delta$ were extracted from S-parameters measurement of a ring resonator [16]. This resonator is composed by a ring with mean radius of 2.95 mm. The width of the microstrip on the Kapton surface is 310 µm to give us a characteristic impedance in the range of 50 Ω. Additionally, a grounded coplanar waveguide (GCPW) to microstrip transition was optimized with the help of HFSS electromagnetic (EM) software to minimize the impedance mismatch. There are two 70 µm gaps at the edges of the ring to couple the resonator with the measurement system, which provides us sufficient coupling to measure the resonator without overload the test equipment (see Fig.5).

The same structures were also modeled using ADS Momentum software [17]. In order to fit measured and simulated data for the entire frequency band, we tuned the dielectric parameters. It is clear that the full 3D Finit Element Method (FEM) used in HFSS software is more accurate than the Method of Moments (MoM) used in ADS Momentum, but in our case, a simulation from 10 to 65 GHz with ADS Momentum is much faster. The correlation between experimental and simulation results is depicted in Fig. 6. Simulated and measured resonant frequencies and quality factors are given in Table 2. The experimental results were obtained by using an Agilent PNA network analyzer and Cascade Microtech GSG probe with a 150 µm pitch. A 2-port on-wafer SOLT calibration method was used. The dielectric properties found for this Kapton polyimide are $\varepsilon_r = 3.2 \pm 0.03$ and tan $\delta = 0.012 \pm 0.004$ within the entire frequency band.

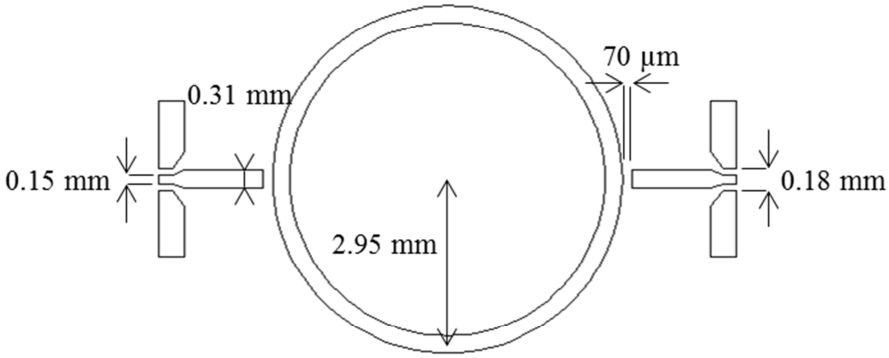


Fig. 5. Ring resonator design

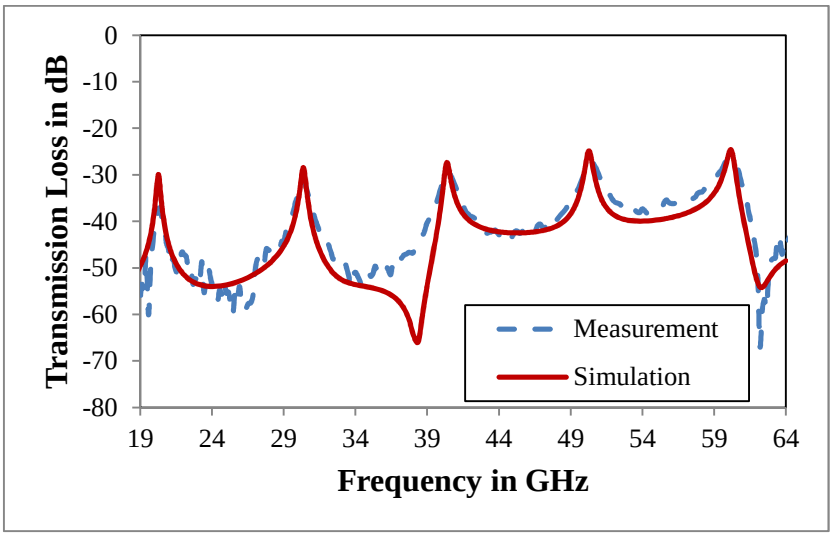


Fig. 6. Simulated and measured insertion loss of the ring resonator.

Table 2. Resonant frequencies & quality factors

| Simulation | | Measurement | |
|---|---|---|---|
| Resonant Frequency | Q factor | Resonant Frequency | Q factor |
| 20.27 | 72.4 | 20.345 | 36.7 |
| 30.36 | 89.3 | 30.265 | 39.1 |
| 40.37 | 98.5 | 40.34 | 42 |
| 50.28 | 104.7 | 50.415 | 44.4 |
| 60.17 | 114.6 | 60.18 | 50.2 |

# IV. DESIGN AND MEASEREMENT OF KAPTON BASED PASSIVE CIRCUITS

## A) Patch antenna

A 60 GHz grounded coplanar waveguide (GCPW) feeding rectangular patch antenna (see Fig. 7 a) was designed, fabricated, and measured on a flexible 127-µm-thick polyimide substrate (Kapton). The GCPW-to-microstrip transition was optimized to reduce the impedance mismatch. The antenna was then characterized in terms of return loss, gain, and radiation pattern.

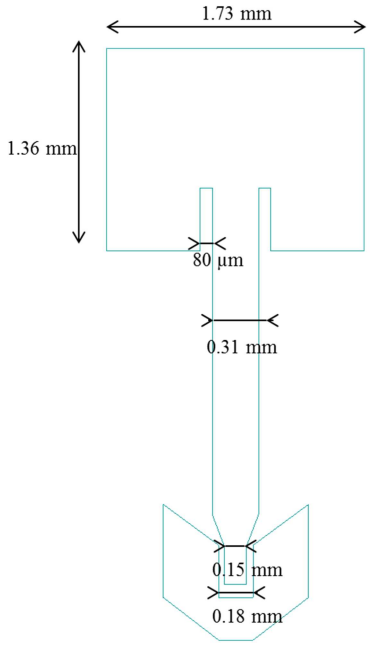


(a)

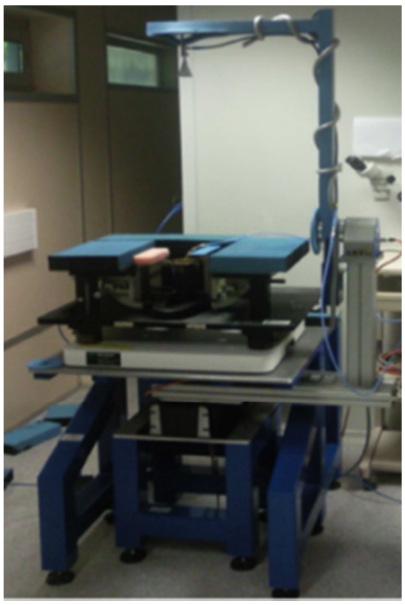

(b)

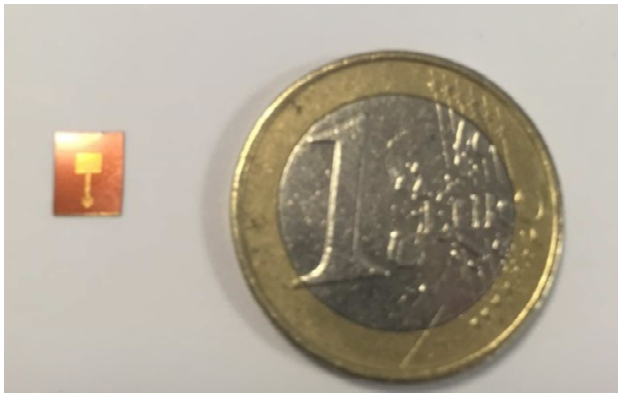

(c)

Fig. 7. (a) 60GHz GCPW feeding rectangular patch antenna; (b) Measurement setup; (c) Manufactured patch antenna on Kapton

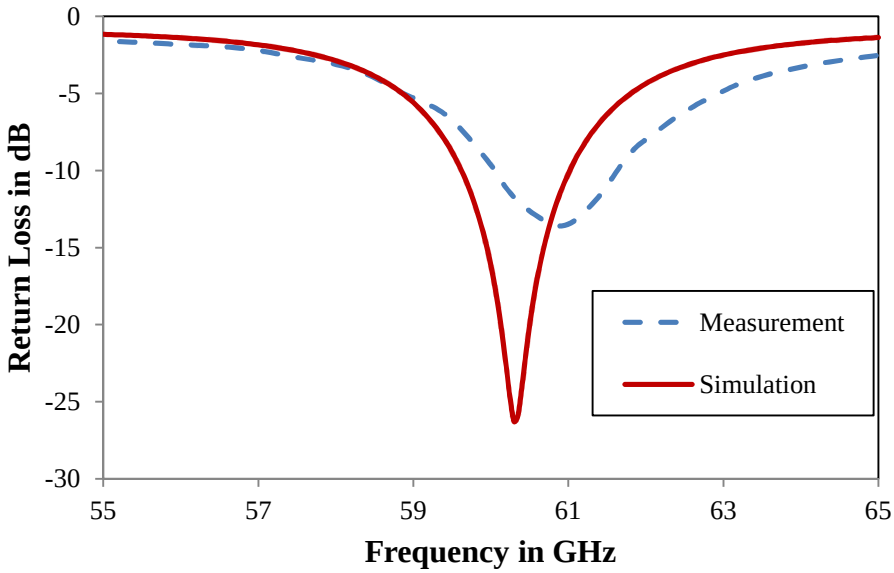


Fig. 8. Simulated and measured return loss of the patch antenna

The simulated and the measured return loss of the patch antenna versus frequency are presented in Fig. 8. The agreement between experiments and simulations is very good: a relative frequency shift of only 0.7% is observed between the simulated (HFSS) and measured results. The difference is due to the uncertainties of the substrate permittivity/permeability value and under/over etching of the conductive patterns. The measured impedance bandwidth, defined by return loss less than -10 dB, is from 60.05 GHz to 61.8 GHz (3% of relative bandwidth).

The far-field radiation pattern and gain measurement were performed with a probe based antenna measurement setup at LAAS (Fig. 7b). The antenna is fed through a 150-µm Ground-Signal-Ground (GSG) probe, and this probe is directly connected to a 65 GHz VNA (Anritsu 37397D) with a flexible V-cable. Dielectric foam from Rohacell was used below the antenna to prevent reflections from the metallic part of the setup. The Antenna Under Test (AUT) was illumined by the field generated by a calibrated VT-15-25-C horn antenna from Vector Telecom.

Under these conditions, a maximum gain of 5 dBi was measured in the perpendicular direction of the antenna at 60.3 GHz. The simulated and measured radiation patterns in the H- and E-plane are given in Fig. 9 and Fig. 10. The difference of gain between simulation and measurement is about 1.7 dB, which may due to insertion loss introduced by the CPW probe and the metallization quality of conductive tracks. The E-plane radiation pattern has a restricted range due to architecture of the measurement setup because the probe was placed in the E-plane. Ripples observed in the E-plane are due to reflection and diffraction effects on the metallic micro-positioner and the probe. The 3dB beamwidth is 56° for the H-plane.

The results demonstrate the quality of fabrication on flexible polyimide substrate and the accuracy of measurement setup for millimeter-wave antenna.

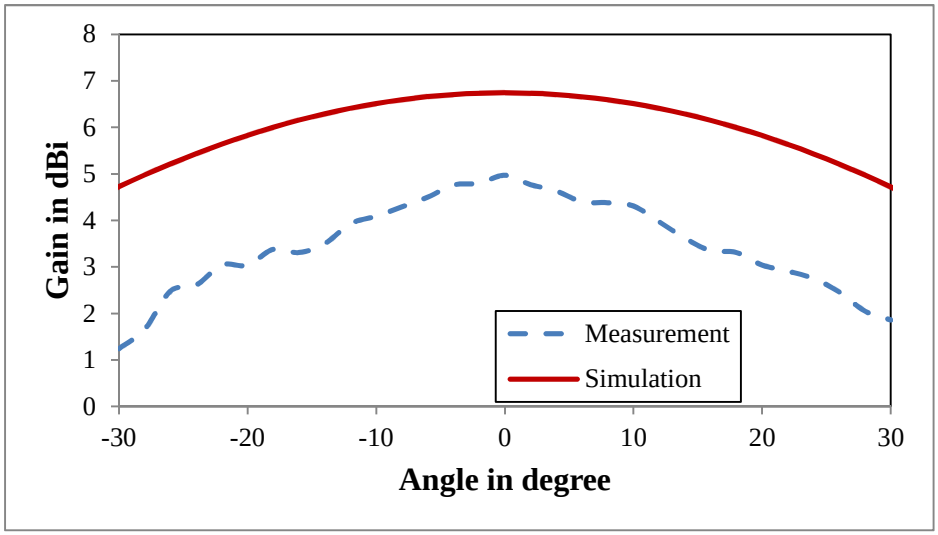


Fig. 9. H-plane radiation patterns of the patch antenna at 60.3 GHz

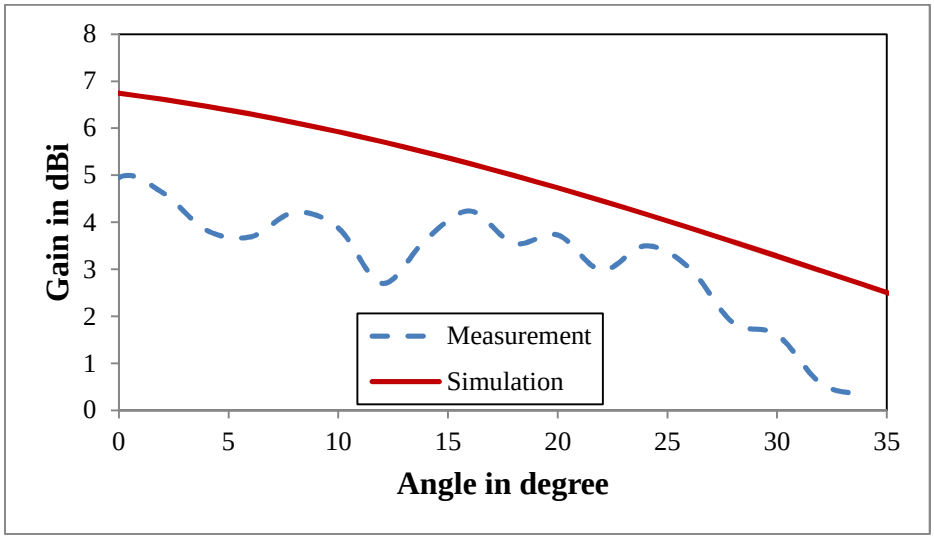


Fig. 10. E-plane radiation patterns of the patch antenna at 60.3 GHz

## B) Cross dipoles array antenna

For the interest of energy harvesting for satellite health monitoring, the cross dipoles array antenna (CDAA) on Kapton polyimide is proposed, which consists of four printed half-wave dipoles arrays on the top side of substrate. As shown in Fig.11, CDAA is a coplanar stripline (CPS) structure. A T-junction CPS-to-microstrip was designed and optimized by using intensive electromagnetic simulations to allow the excitation of the CDAA by a microstrip and the proper connection with a K “end launch” connector from Southwest for measurement purposes [18].

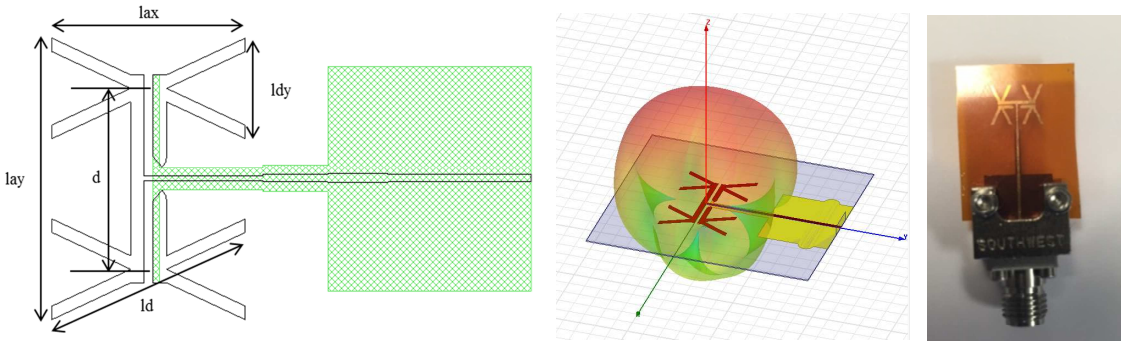


(a) (b) (c)

Fig. 11. a) Cross dipoles array antenna: top view of the layout (the bottom layout is represented in filled with green trellis); b) Simulation model; c) manufactured antenna

Table 3. Cross dipoles array antenna dimensions

| Band | lax (mm) | lay (mm) | d (mm) | Ld (mm) | Ldy (mm) |
|---|---|---|---|---|---|
| **Ku** | 8.5 | 12.42 | 8 | 93.18 | 4.42 |
| **K** | 5.7 | 7.5 | 4.5 | 6.26 | 3 |

Two CDAAs operating in $K_u$ and K band are fabricated and measured respectively, their dimensions are summarized in Table 3. S-parameter measurement and simulation results are reported in Fig. 12 and Fig. 13. One can see a large impedance bandwidth is obtained (measured at S11 = -10 dB) for two proposed antennas, 15.45 GHz to 19.35GHz for the $K_u$ band CDAA (22% of relative bandwidth), and 21.7GHz to 25.7GHz for the K band CDAA (17% of relative bandwidth).

The radiation pattern characterizations were performed in an anechoic chamber. Fig. 14 and Fig. 15 report the measured and simulated radiation patterns in two orthogonal planes at 17 GHz for the $K_u$ band CDAA. Fig. 16 and Fig. 17 report the measured and simulated radiation patterns at 22 GHz for the K band CDAA. We note that the simulation results were obtained in HFSS and the "end-launch" connector was not included in the model. The difference of gain between measurement and simulation is about 2.7 dB may due to (i) the losses introduced by the "end-launch" connector (estimated to be in the range of 1 dB); (ii) the assembling mechanical process for connecting the Kapton structure to the connector that can lead to an imperfect contact; (iii) the skin effect. Metallization layers are composed by: (a) adherent layer of Ti about 50 nm; (b) cooper layer (thickness: 500 nm); (c) gold layer (thickness: a few nanometers). As mentioned in section II, the skin depth of copper at 20 GHz is 460 nm which is comparable with the total metal thickness of 600 nm, thus unexpected RF losses may occur. The ripples observed in the YOZ plane (phi = 90°) are due to reflection and diffraction effects on the connector and the coaxial cable. The 3dB beamwidth is 52° in the XOZ plane and 65° in the YOZ plane for the $K_u$ band CDAA at 17 GHz. For the K band CDAA, The 3dB beamwidth is 58° in the XOZ plane and 62° in the YOZ plane at 22 GHz. As depicted from Fig. 12 to Fig. 17, the proposed CDAAs are wideband antennas (22% of relative bandwidth in Ku band and 17% of relative bandwidth in

K band). The radiation pattern do not change significantly in the relative bandwidth and the measured maximum gain is about 4.3 dBi (included the losses added by the end lunch connector and the associated mounting process and by CPS-to-microstrip T junction). We note that the gain can be increased by 3dB if a metallic plate acting as reflector is properly putted below the CDAA.

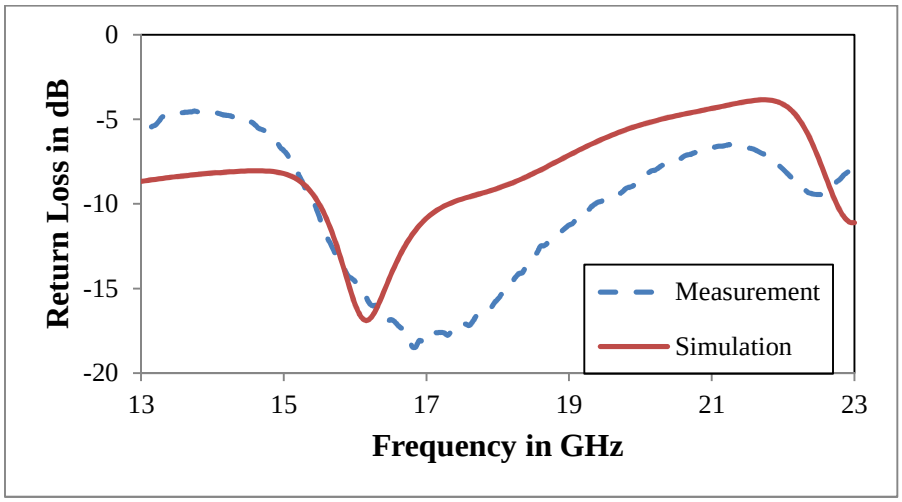


Fig. 12. Simulated and measured return loss of the $K_u$ band CDAA

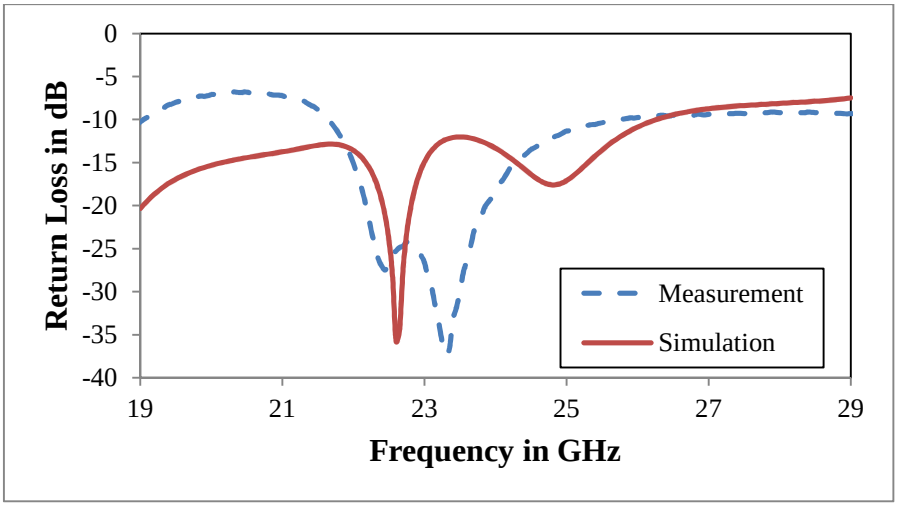


Fig. 13. Simulated and measured return loss of the K band CDAA

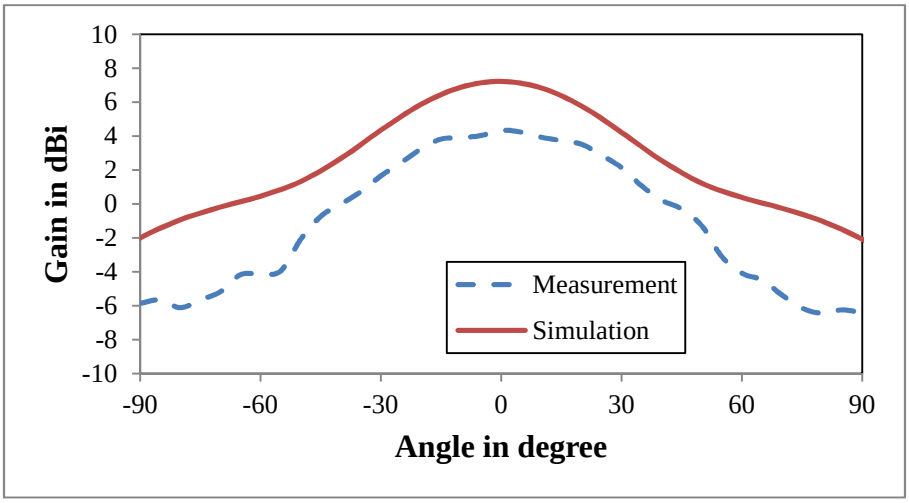


Fig. 14. XOZ plane (phi = 0°) radiation patterns of the $K_u$ band CDAA at 17 GHz

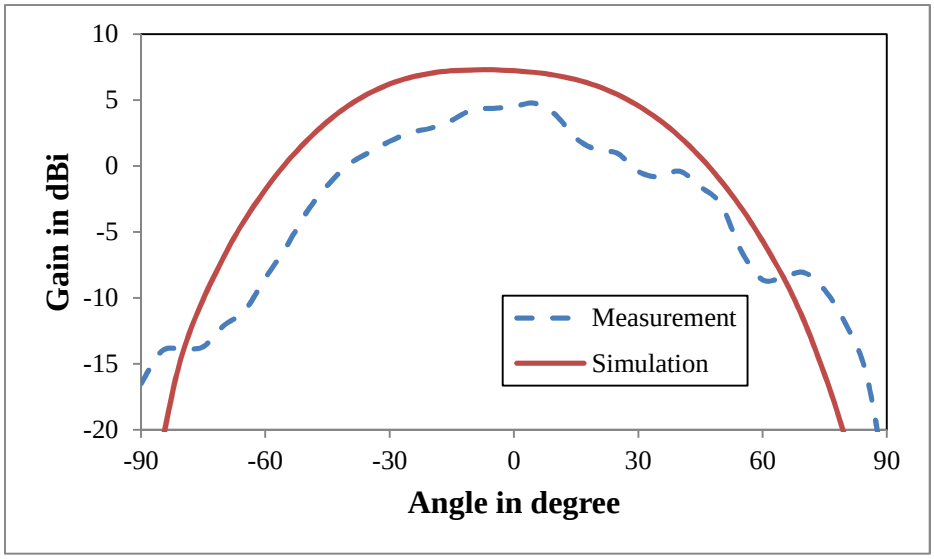


Fig. 15. YOZ plane (phi = 90°) radiation patterns of the $K_u$ band CDAA at 17 GHz

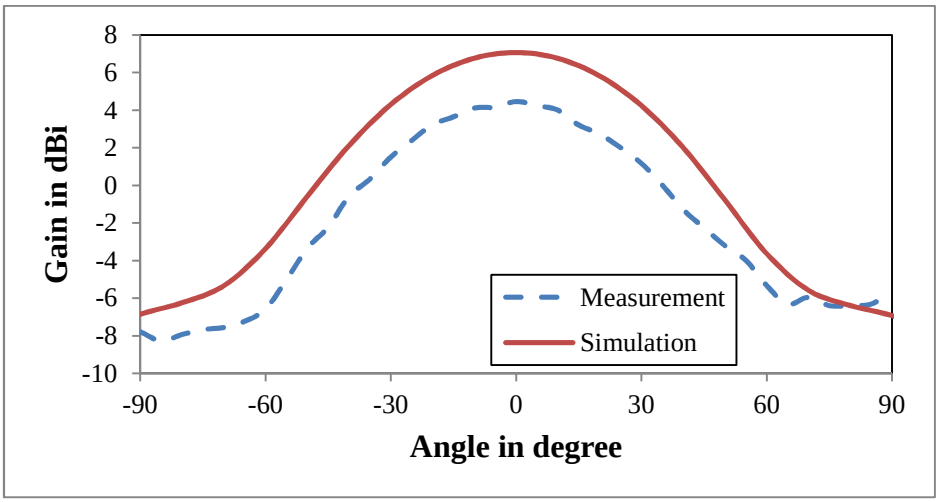


Fig. 16. XOZ plane (phi = 0°) radiation patterns of the K band CDAA at 22 GHz

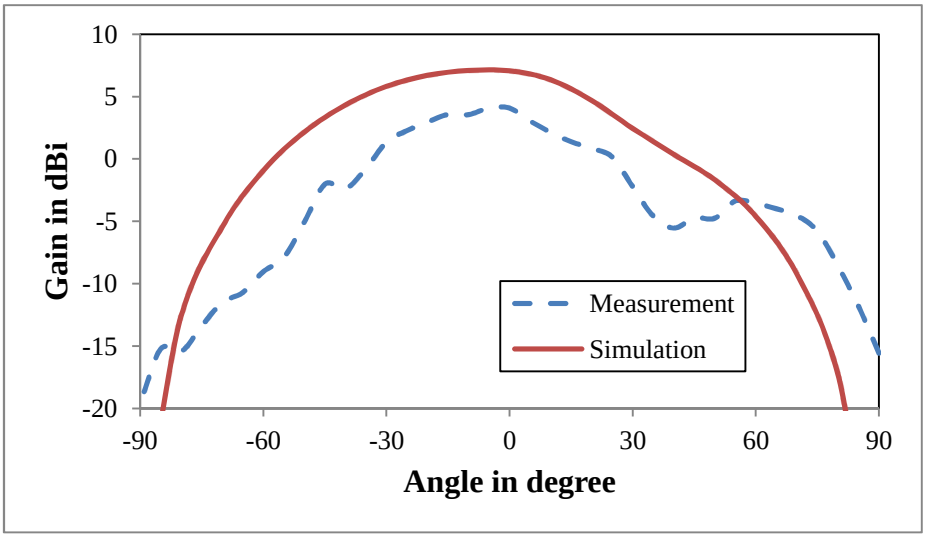


Fig. 17. YOZ plane (phi = 90°) radiation patterns of the K band CDAA at 22 GHz

## C) Cross slot dipole antenna

Inspired by the design of CDAAs at $K_u$ band and K band, and the Babinet's principle which relates the radiated field and impedance of a slot antenna to a printed (strip) antenna, a first prototype of Crossed Slot Dipole Antenna (CSDA) in V band is proposed shown in Fig. 18. The antenna is designed on a 127-µm thick Kapton with a dielectric constant 3.2 and a loss tangent 0.006. CPW feed dimensions of S = 170 µm and G = 12 µm were selected corresponding to the 50 Ohm GSG probe. The slot length L is fixed to 1.3 mm (quarter wavelength for 60 GHz) for the simulation, the slot width w, the stub length d and the angle between slots α were set to 40 µm, 0.69 mm and 45° as default respectively.

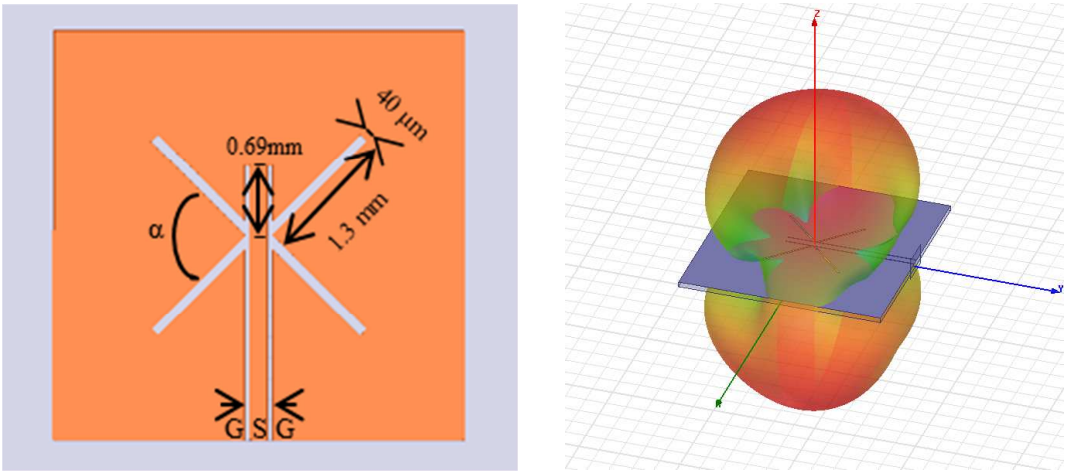


(a) (b)

Fig. 18. a) Design of crossed slot dipole antenna; b) Simulation model

Fig. 19 shows the simulated return loss. The center frequency is 60.2 GHz, and the -10 dB bandwidth is from 58.2 GHz to 62.05 GHz (6% of relative bandwidth). The antenna radiation

patterns were also presented in Fig. 20, a peak antenna gain of 4.02 dB is obtained at 60.2 GHz.

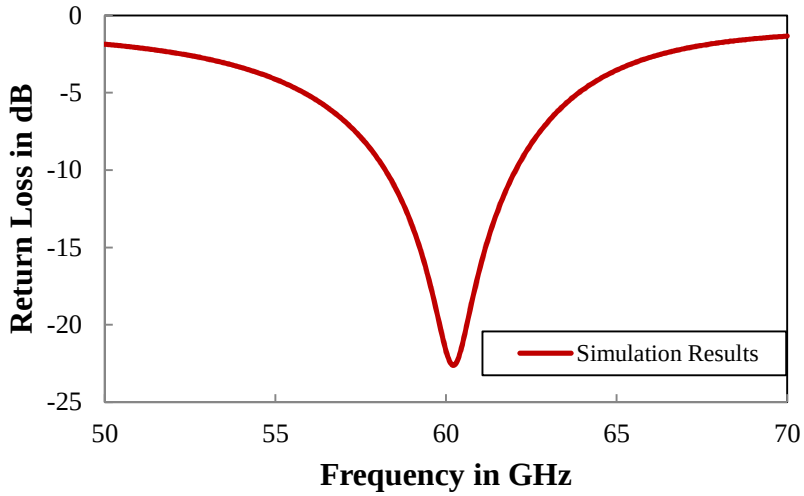


Fig. 19. Simulated return loss of the cross slot dipole antenna

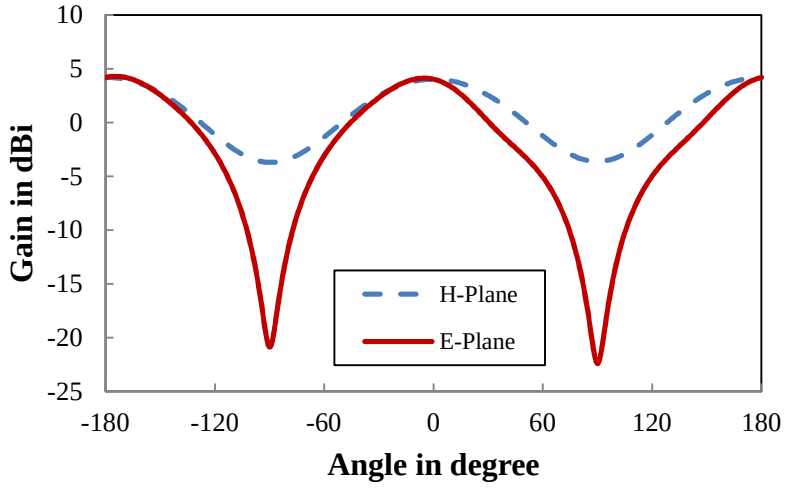


Fig. 20. Simulated (HFSS) radiation patterns in E-Plane and H-Plane at 60.2 GHz

A parametric study for the angle between slots is shown in Table 4. It is seen that when the angle α increase, the peak antenna gain decrease along with a larger half power beamwidth (HPBW) on H-plane. This phenomenon can be explained by the increase of the coupling effect when the slots approach each other.

As demonstrated by the simulation, CSDA has interesting performances in 60 GHz band. This antenna has no ground plane and in V band its performances (input matching and radiation pattern) can be impacted by the surrounding environment placed behind the antenna (the metallic chuck of the probe station used for S-parameters measurement or the dielectric

supporting plate of the antenna setup shown in Fig. 7 b). In order to avoid such issues and obtain a good correlation between simulation and measurements two solutions can be envisaged: (i) redesign this antenna by using a reflector/ground plane properly positioned behind the antenna and (ii) re-simulate the antenna taking into account a representative 3D model of the surrounding environment. Both solutions are time consuming and were not implemented before the submission of this paper.

Table 4. Study of angle α effect on radiation

| α (°) | fc (GHz) | Return Loss (dB) | Maximum Gain | HPBW (°) |
|---|---|---|---|---|
| **40** | 59.7 | -21.09 | 4.14 | 82 |
| **45** | 60.2 | -22.76 | 4.02 | 86 |
| **50** | 61.15 | -27.48 | 40.8 | 90 |

## V. INTEGRATION ASSEMBLY TEST

For the purpose of integration of different components on Kapton polyimide, different dummy circuits are realised and mounted by using a well matured flip chip technique established in LAAS-CNRS as shown in Fig. 21 [19]. To measure the quality of the contacts, four probe method was used to characterize the bumps resistivity as shown in Fig. 22. A resistance about 10 mΩ was measured for the Au bump, which proves a very good DC contact has been achieved by using this technique.

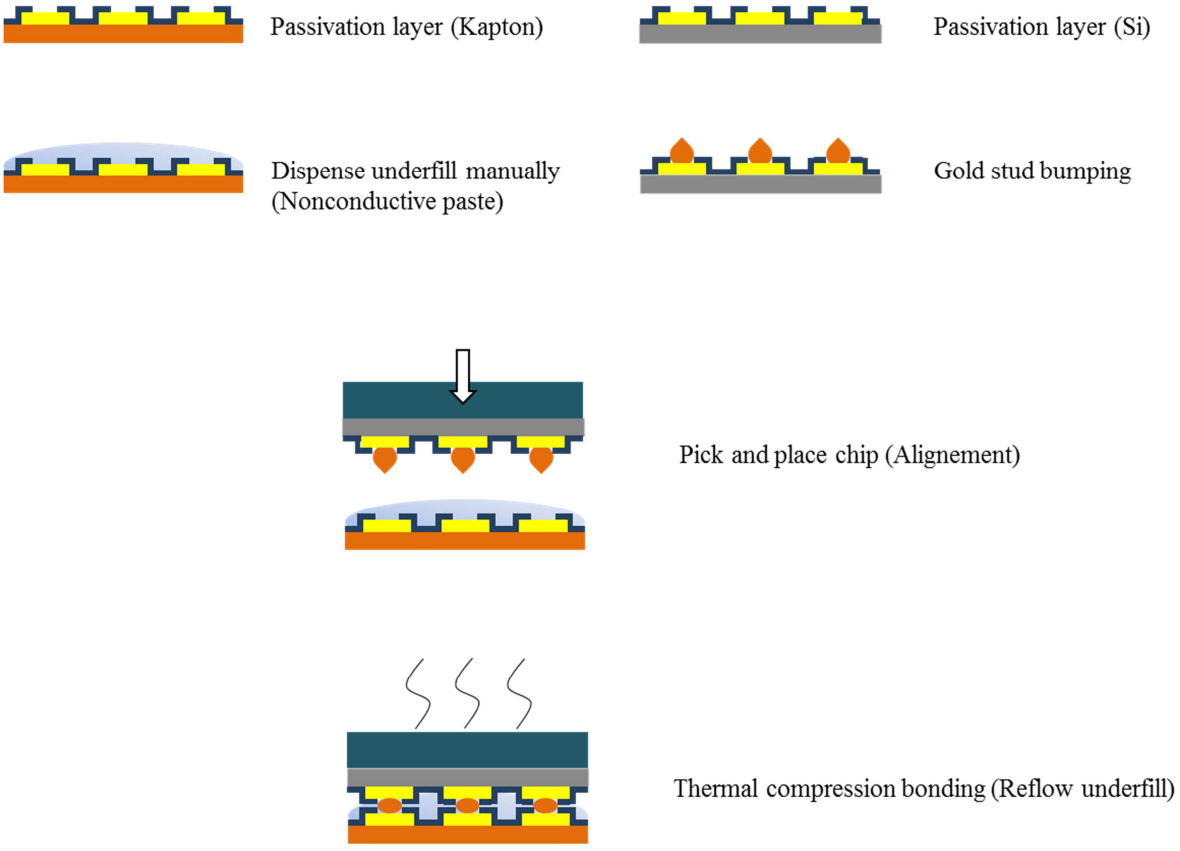


Fig. 21 Description of flip chip process

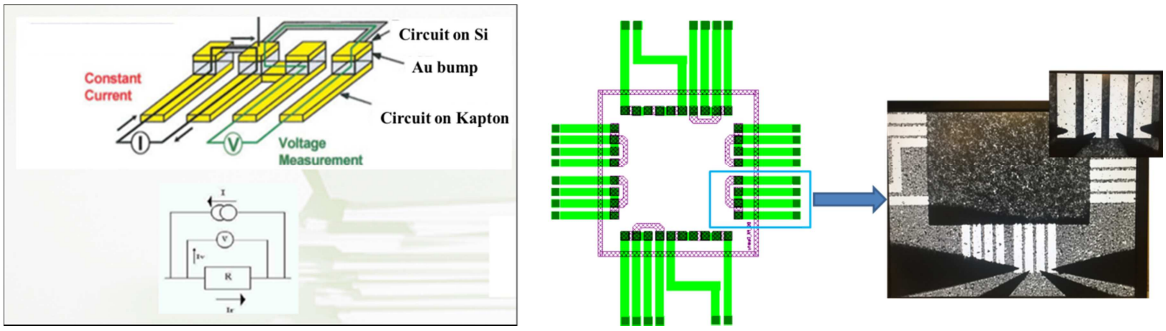


Fig. 22. Four probe method resistivity measurement

The presented Kapton supported technology can be used to develop millimeter wave circuits by heterogeneous integration for the implementation of wireless sensors network (including autonomous wireless sensors by using energy harvesting or wireless power transfer techniques). The RF power used for that application is generally very low and is subject to regulation. For example in V-band, the EIRP limitations for operation in the US limits [20] the EIRP at 40 dBm (conducted power up to 27 dBm). In Europe [21], stipulates a maximum conducted power of less than +10 dBm. To the author best knowledge, these (maximum) authorized power levels are not critical for Kapton technology that has a very good thermal behavior.

## VI. Conclusion

In this work, we demonstrate the feasibility of manufacturing microwave passive circuits at high frequency on a commercially available polyimide Kapton substrate through a traditional photolithography process. A 60 GHz patch antenna has been designed, fabricated, and measured to validate our technology. Crossed dipoles array antenna at Ku band and K band for energy harvesting have also been designed, fabricated and measured. Simulation results agree well with the experimental results, only 0.7% of frequency shift is observed for return loss of 60 GHz patch antenna, 6.2% and 3.1% for $K_u$ and K band CDAA respectively. Future measurement for the cross slot dipole antenna will be carry on. The results of flip chip test are one step further towards a heterogeneous integration on flexible substrate of different components for autonomous wireless sensor nodes using wireless power transfer.

## REFERENCES

[1] Wong, W.S.; Salleo, A.: Flexible Electronics: Materials and Applications, Springer Publishing Company, Incorporated, 2009.

[2] Vyas, R.; Rida, A.; Bhattacharya, S.; Tentzeris, M.M.: Liquid Crystal Polymer (LCP): The ultimate solution for low-cost RF flexible electronics and antennas, in Antennas and Propagation Society International Symp., 2007, 1729-1732.

[3] Printing Technology for Flexible Substrates, InterLingua Publishing, 2006.

[4] Hettak, K.; Petosa, A.; James, R.: Flexible plastic-based inkjet printed CPW fed dipole antenna for 60 GHz ISM applications, in Antennas and Propagation Society International Symp., 2014, 328-329.

[5] Bisognin, A.; Thielleux, J.; Wei Wei; Titz, D.; Ferrero, F.; Brachat, P.; Jacquemod, G.; Happy, H.; Luxey, C.: Inkjet Coplanar Square Monopole on Flexible Substrate for 60-GHz Applications, Antennas and Wireless Propagation Letters, IEEE, 13(2014), 435-438.

[6] http://www.dupont.com/content/dam/assets/products-and-services/membranes-films/assets/ DEC-Kapton-summary-of-properties.pdf.

[7] Shaker, G.; Safavi-Naeini, Safieddin; Sangary, N.; Tentzeris, M.M.: Inkjet Printing of Ultrawideband (UWB) Antennas on Paper-Based Substrates, Antennas and Wireless Propagation Letters, IEEE , 10(2011), 111-114.

[8] Chauraya, A.; Whittow, W.G.; Vardaxoglou, J.C.; Yi Li; Torah, R.; Kai Yang; Beeby, S.; Tudor, J.: Inkjet printed dipole antennas on textiles for wearable communications, Microwaves, Antennas & Propagation, IET , 7(9)(2013), 760-767.

[9] Swaisaenyakorn, S.; Young, P.R.; Shkunov, M.: Characterization of ink-jet printed CPW on Kapton substrates at 60 GHz, in Antennas and Propagation Conf. LAPC, Loughborough, 2014, 676-678.

[10] Belhaj, M.M.; Wei Wei; Pallecchi, E.; Mismer, C.; Roch-jeune, I.; Happy, H.: Inkjet printed flexible transmission lines for high frequency applications up to 67 GHz, in European Microwave Conf., EuMC 2014, 1528-1531.

[11] Singh, M.; Haverinen, H.M.; Dhagat,P.; Jabbour, G.E.: Inkjet printing—process and its applications, Advanced materials, 22(6)(2010),673-685.

[12] Ahmed, S.; Tahir, F.A.; Shamim, A.; Cheema, H.M.: A Compact Kapton-based Inkjet Printed Multiband Antenna for Flexible Wireless Devices, Antennas and Wireless Propagation Letters, IEEE, 99(2015),1-1.

[13] Aziz, M.A.; Roy, S.; Berge, L.A.; Irfanullah; Nariyal, S.; Braaten, B.D.: A conformal CPW folded slot antenna array printed on a Kapton substrate, Antennas and Propagation EUCAP, 2012, 159-162.

[14] Jatlaoui, M.M.; Dragomirescu, D.; Charlot, S.; Pons, P.; Aubert, H.; Plana, R.: 3D heterogeneous integration of wireless communicating nano-sensors on flexible substrate, Proc. SPIE 7821, Advanced Topics in Optoelectronics, Microelectronics, and Nanotechnologies, 2010.

[15] http://www.ansys.com/Products/Simulation+Technology/Electronics/Signal+Integrity/ANSYS+HFSS

[16] Thompson, D.; Tantot, O.; Jallageas, Hubert; Ponchak, G.E.; Tentzeris, M.M.; Papapolymerou, J.: Characterization of liquid crystal polymer (LCP) material and transmission lines on LCP substrates from 30 to 110 GHz, Microwave Theory and Techniques, IEEE Trans., 52(4)(2004), 1343-1352.

[17] http://www.keysight.com/en/pc-1887116/momentum-3d-planar-em-simulator?nid=-33748.0&cc=US&lc=eng.

[18] Takacs, A.; Aubert, H.; Fredon, S.; Despoisse, L.: Design and Characterization of Effective Antennas for K-band Rectennas, in Antennas and Propagation EUCAP, 2015, 1-4.

[19] Jatlaoui, M.M.; Dragomirescu, D.; Ercoli, M.; Krämer, M.; Charlot, S.; Pons, P.; Aubert, H.; Plana, R.: Wireless communicating nodes at 60 GHz integrated on flexible substrate for short-distance instrumentation in aeronautics and space, International Journal of Microwave and Wireless Technologies, 4(2012), 109-117.

[20] https://www.fcc.gov/document/part-15-rules-unlicensed-operation-57-64-ghz-band.

[21] http://www.erodocdb.dk/docs/doc98/official/pdf/Rec0901.pdf.